WELDING RESEARCH

SUPPLEMENT TO THE *WELDING JOURNAL*, JULY 2005
**Sponsored by the American Welding Society and the Welding Research Council**

# Reliable Calculations of Heat and Fluid Flow during Conduction Mode Laser Welding through Optimization of Uncertain Parameters

*A deterministic approach is proposed to improve reliability of heat transfer and fluid flow calculations*

BY A. DE AND T. DebROY

ABSTRACT. During conduction mode laser beam welding, the quality of numerical simulation of heat transfer and fluid flow in the weld pool is significantly affected by the uncertainty in the values of absorptivity, effective thermal conductivity, and effective viscosity that cannot be easily prescribed from fundamental principles. Traditionally, values of these parameters are either prescribed based on experience or adjusted by trial and error. This paper proposes a deterministic approach to improve reliability of heat transfer and fluid flow calculations. The approach involves evaluation of the optimized values of absorptivity, effective thermal conductivity, and effective viscosity during conduction mode laser beam welding from a limited volume of experimental data utilizing an iterative multivariable optimization scheme and a numerical heat transfer and fluid flow model. The optimization technique minimizes the error between the predicted and the measured weld dimensions by considering the sensitivity of weld dimensions with respect to absorptivity, effective thermal conductivity, and effective viscosity. Five sets of measured weld pool dimensions corresponding to five different welding conditions were utilized for the optimization. However, the procedure could identify the optimized values of the three uncertain parameters even with only three sets of measured weld pool dimensions.

*A. DE (amit@me.iitb.ac.in) is with the Mechanical Engineering Department, IIT Bombay, Mumbai, India. T. DebROY (debroy@psu.edu) is with the Department of Material Science and Engineering, The Pennsylvania State University, University Park, Pa.*

## Introduction

Since the temperature and velocity fields in the weld pool are difficult to measure experimentally (Refs. 1–7), these important variables are often estimated by numerically solving the equations of conservation of mass, momentum, and energy. In recent years, the numerically computed temperature fields have been utilized to estimate weld pool dimensions (Refs. 4–7) and understand weld metal phase composition (Refs. 8–11), grain structure (Refs. 10, 11), inclusion structure (Refs. 12–14), and weld metal composition changes owing to both vaporization of alloying elements (Refs. 15, 16) and dissolution of gases (Refs. 17, 18).

The transport phenomena-based numerical models have been continually updated to include more detailed and realistic descriptions of component physical processes for simple(Refs. 19–22) as well as for complex weld joint geometries (Ref. 23). In recent years, these models have become relatively easy to use because of advances in computational hardware and software. However, these powerful numerical heat transfer and fluid flow models have not found widespread use in manufacturing or design applications. An important difficulty is the uncertainty involved in specifying some of the necessary input variables such as absorptivity, effective thermal conductivity, and effective viscosity. Although the time-tested physical laws such as the equations of conservation of mass, momentum, and energy provide a reliable phenomenological framework for calculations, the reliability of the numerical process models greatly depends on the accuracy of several input parameters.

**KEY WORDS**

Laser
Laser Beam Welding
Heat Transfer
Fluid Flow
Conduction Mode

Many input parameters necessary for the numerical simulation of heat transfer and fluid flow in conduction-mode linear laser beam welding can be readily specified. These include welding speed, beam power, beam diameter, and thermophysical properties of the material being welded (Refs. 19, 24). However, the values of absorptivity, effective thermal conductivity and effective viscosity cannot be specified from fundamental principles (Refs. 2, 24–30). For example, absorptivity depends on the chemical composition of the substrate, the surface finish, laser mode, and the prevailing temperature distribution on the weld pool. As a result, the absorption coefficient cannot be estimated theoretically with high reliability. However, an accurate value of absorptivity is critical for the dependable estimation of the rate of heat absorption. Similarly, appropriate values of effective thermal conductivity and effective viscosity are needed for the reliable modeling of the high rates of transport of heat, mass, and momentum in weld pools with strong fluctuating velocities (Ref. 25). Enhanced values of liquid thermal conductivity and viscosity have been frequently used to take into account the effects of the fluctuating

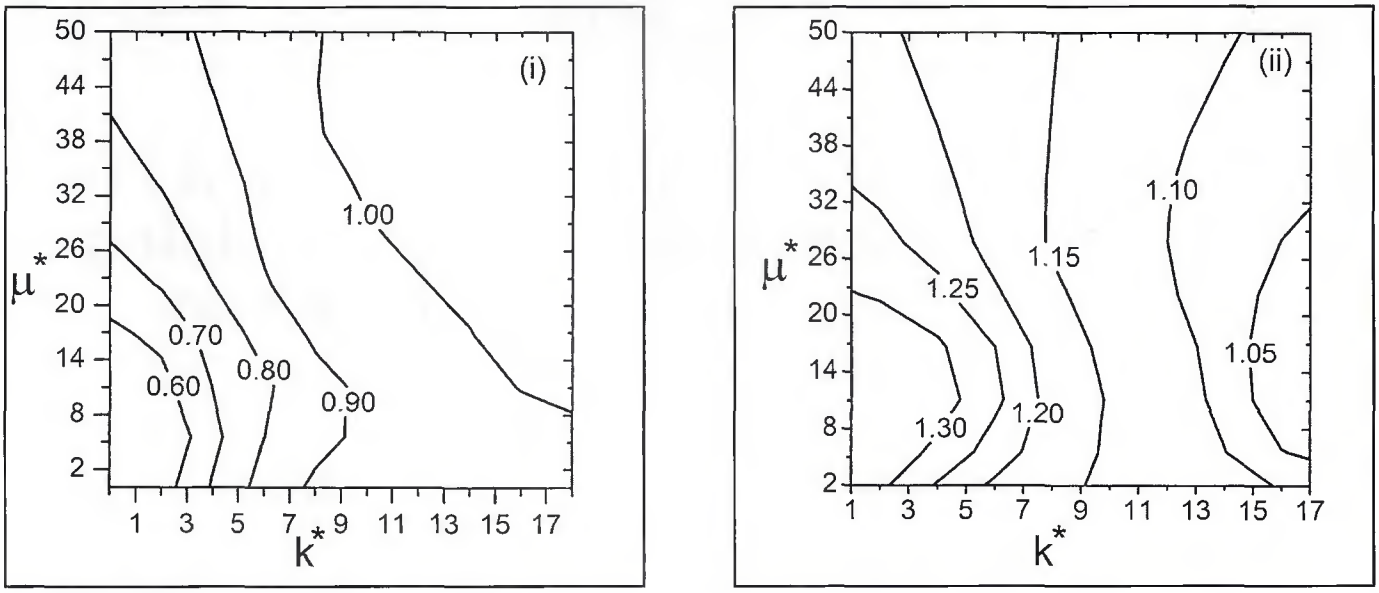


*Fig. 1 — Influence of k* and μ* on (i) $p_m^*$ and (ii) $w_m^*$ with assumed absorptivity (η) of 0.30. Welding parameters: P = 3200 W, v = 3.33 mm/s ($N_{HI}$ = 21.90).*

**Table 1 — Measured Weld Dimensions, Welding Parameters (Ref. 24), and Heat Input Index**

| Data Set Index | Laser Power (W) | Weld Velocity (mm.s$^{-1}$) | Spot Radius (mm) | $N_{HI}$ | Weld Penetration (mm) | Weld Width (mm) |
|---|---|---|---|---|---|---|
| 1 | 3500 | 8.33 | 1.3 | 9.67 | 1.00 | 4.00 |
| 2 | 5000 | 8.33 | 1.3 | 14.97 | 1.25 | 5.25 |
| 3 | 3200 | 3.33 | 1.4 | 21.90 | 1.75 | 4.00 |
| 4 | 4800 | 3.33 | 1.4 | 32.90 | 2.50 | 6.00 |
| 5 | 5000 | 3.33 | 1.3 | 34.53 | 2.25 | 6.75 |

**Table 2 — Chemical Composition (wt-%) of High-Speed Steel Used for Welding Experiments[a]**

| C | Cr | W | Mo | V | Co | Mn |
|---|---|---|---|---|---|---|
| 0.92 | 3.88 | 6.08 | 4.9 | 1.73 | 0 | 0.26 |
| Si | S | Ni | P | Cu | Al | Fe |
| 0.23 | 0.001 | 0.24 | 0.024 | 0.20 | 0.019 | Bal. |

(a) for data set index 1, 2, and 5 (Ref. 24).

components of velocities in the weld pool. In some cases, the two-equation k-ε turbulence model has also been used in estimating the effective viscosity and effective thermal conductivity in the weld pool (Refs. 26–28). However, the two-equation k-ε turbulence model contains several empirical constants that were originally estimated from parabolic fluid flow data in large systems. As a result, its applicability for the recirculating flow in small scale systems has not been adequately tested. Since the effective thermal conductivity and viscosity depend on the turbulent kinetic energy and other properties of convection, these parameters are system properties (Refs. 1, 2, 24–30) and their values depend on welding conditions, particularly the heat input.

The values of effective viscosity and thermal conductivity have been determined in this work as a function of heat input from a limited volume of measured weld pool dimensions for conduction mode linear laser beam welding (Ref. 24) utilizing an optimization algorithm and a numerical heat transfer and fluid flow model. In contrast with the effective viscosity or the effective thermal conductivity, the laser beam absorption coefficient is a materials property. Although it varies with temperature, the extent of the variation is normally much smaller than those of the effective thermal conductivity or the effective viscosity. It has been taken as a constant in this work for simplicity. The optimization algorithm minimizes the error between the predicted and the experimentally observed penetrations and the weld widths by considering the sensitivity of the computed weld pool dimensions with respect to the absorptivity, effective thermal conductivity, and effective viscosity. The sensitivity terms are calculated by running the heat transfer and fluid flow model several times for each measurement considering small changes in the absorptivity, effective thermal conductivity, and effective viscosity (Refs. 29, 30).

The approach determines the values of absorptivity, effective viscosity and thermal conductivity in an iterative manner starting from a set of their initial guessed values. In order to include the effects of laser power, spot diameter, and welding speed into one convenient variable during optimization, a nondimensional heat input variable, $N_{HI}$, is defined as

$$N_{HI} = \frac{\dfrac{P}{\pi r_{b}^{2} \cdot v}}{\rho C_{PS}(T_L - T_a) + \rho L} \qquad (1)$$

where P is the laser power (W), $r_b$ the spot radius (m), v the welding velocity (m·s$^{-1}$), $C_{PS}$ the specific heat of the solid metal (J·kg$^{-1}$·K$^{-1}$), ρ the density (kg·m$^{-3}$), L the latent heat of fusion (J·kg$^{-1}$) and $T_L$ and $T_a$ are the liquidus and ambient temperatures (K), respectively. In Equation 1, the numerator represents the available laser power per unit volume and the denominator depicts the enthalpy required to heat a unit volume of metal from ambient temperature to liquidus temperature. The numerator in Equation 1 when multiplied by the absorptivity, η, provides the absorbed heat per unit volume. The optimization approach identifies a single value of absorptivity and a linear trend of effective thermal conductivity and effective viscosity with $N_{HI}$ from a limited volume of measurements.

The work presented in this manuscript represents a significant improvement over the previous (Refs. 31–35) reverse model-

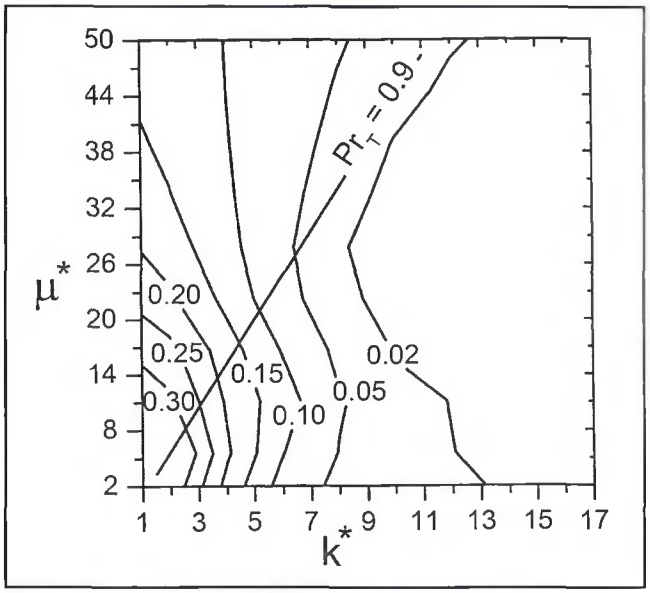


*Fig. 2 — Influence of k* and μ* on O(f) with assumed absorptivity (η) of 0.30. Welding parameters: P = 3200 W, v = 3.33 mm/s ($N_{HI}$ = 21.90).*

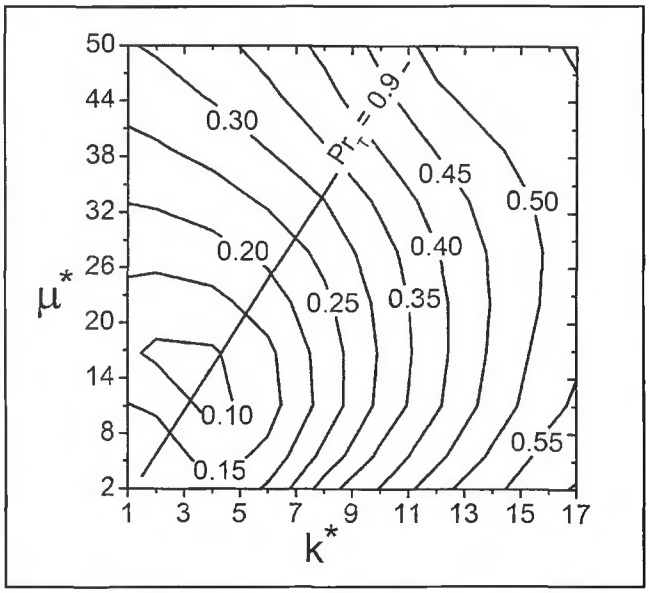


*Fig. 3 —Influence of k* and μ* on O(f) with assumed absorptivity (η) of 0.30. Welding parameters: P = 5000 W, v = 8.33 mm/s ($N_{HI}$ = 14.97).*

ing work in welding reported in the literature. First, unlike the previous efforts, a well-tested, three-dimensional numerical heat transfer and fluid flow model is used to compute the weld pool geometry. This is significant, because previous research has shown the importance of convective heat transfer in the weld pool. Second, the model input and the computed weld pool geometry are related by a rigorous phenomenological framework of the conservation of mass, momentum, and energy used in the optimization algorithm. The optimized values of absorptivity, effective thermal conductivity, and effective viscosity were tested by comparing the computed weld dimensions with the corresponding experimentally determined values (Ref. 4).

The effect of volume of data on the outcome of the optimization was examined. First, the optimization was done using five sets of measured weld pool dimensions. Second, the optimization was also carried out with only three measured data sets of weld pool dimensions. The optimized values of the uncertain variables were almost identical in both cases.

## Heat Transfer and Fluid Flow Simulation

Table 1 depicts five sets of measurements of weld dimensions and the corresponding welding parameters that have been used in the present investigation. The chemical compositions of the steels used are presented in Tables 2 and 3. The steel compositions conform to two different grades of high-speed steel (Ref. 24). The thermophysical properties of these steels are given in Tables 4 and 5. The flow of liquid metal in the weld pool in a three-dimensional cartesian coordinate system is represented by the following momentum conservation equation (Refs. 4, 21, 22, 36):

$$\rho\frac{\partial u_j}{\partial t}+\rho\frac{\partial\left(u_i u_j\right)}{\partial x_i}=\frac{\partial}{\partial x_i}\left(\mu\frac{\partial u_j}{\partial x_i}\right)+S_j \qquad (2)$$

where ρ is the density, t is the time, $x_i$ is the distance along the i = 1, 2 and 3 directions, $u_j$ is the velocity component along the j direction, μ is the effective viscosity, and $S_j$ is the source term for the $j^{th}$ momentum equation and is given as (Refs. 21, 22)

$$S_j=-\frac{\partial p}{\partial x_j}+\frac{\partial}{\partial x_j}\left(\mu\frac{\partial u_j}{\partial x_j}\right)-C\left(\frac{\left(1-f_L\right)^2}{f_L^{\,3}+B}\right)u_j-\rho U\frac{\partial u_i}{\partial x_i}+Sb_j \qquad (3)$$

where p is the pressure, $f_L$ is the liquid fraction, B is a constant introduced to avoid division by zero, C (=$1.6\times10^4$) is a constant that takes into account mushy zone morphology and $S_{bj}$ represents both the electromagnetic and buoyancy source terms. The third term on the right-hand side (RHS) represents the frictional dissipation in the mushy zone according to the Carman-Kozeny equation for flow through a porous media (·Refs. 37, 38). The pressure field was obtained by solving the following continuity equation simultaneously with the momentum equation

$$\frac{\partial\left(\rho u_i\right)}{\partial x_i}=0 \qquad (4)$$

**Table 3 — Chemical Composition (wt-%) of High-Speed Steel Used for Welding Experiments[a]**

| C | Cr | W | Mo | V | Co | Mn |
|---|---|---|---|---|---|---|
| 0.21 | 0.21 | <0.05 | 0.05 | <0.02 | <0.05 | 1.52 |
| Si | S | Ni | P | Cu | Al | Fe |
| 0.36 | 0.006 | 0.14 | <0.005 | 0.14 | 0.01 | Bal. |

(a) for data set index 3 and 4 (Ref. 24).

**Table 4 — Data Used for Calculations of Temperature and Velocity Fields[a]**

| Physical Property | Value |
|---|---|
| Liquidus temperature, $T_L$ (K) | 1700.0 |
| Solidus temperature, $T_S$ (K) | 1480.0 |
| Ambient temperature, $T_a$ (K) | 293.0 |
| Density of liquid metal, ρ (kg/m³) | $8.1\times10^3$ |
| Thermal conductivity of solid, $k_s$ (W m$^{-1}$ K$^{-1}$) | 25.08 |
| Thermal conductivity of liquid, $k_L$ (W m$^{-1}$ K$^{-1}$) | 25.08 |
| Specific heat of solid, $C_{PS}$ (J kg$^{-1}$ K$^{-1}$) | 711.0 |
| Specific heat of liquid, $C_{PL}$ (J kg$^{-1}$ K$^{-1}$) | 711.0 |
| Temperature coefficient of surface tension, dγ/dT (N m$^{-1}$ K$^{-1}$) | $-0.5\times10^{-3}$ |
| Coefficient of thermal expansion, β (K$^{-1}$) | $1.5\times10^{-6}$ |
| Viscosity of molten iron at 1823 K, $\mu_{fl}$ (kg.m$^{-1}$s$^{-1}$) | $6.7\times10^{-3}$ |

(a) for data set index 1, 2, and 5 (Ref. 24).

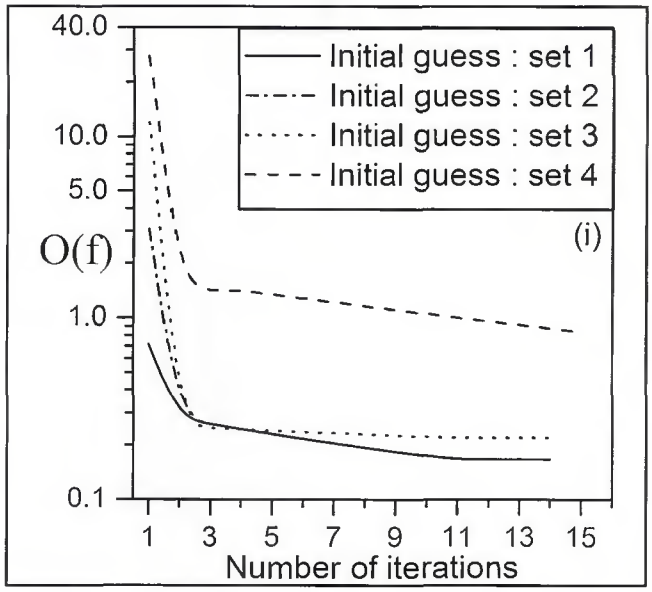


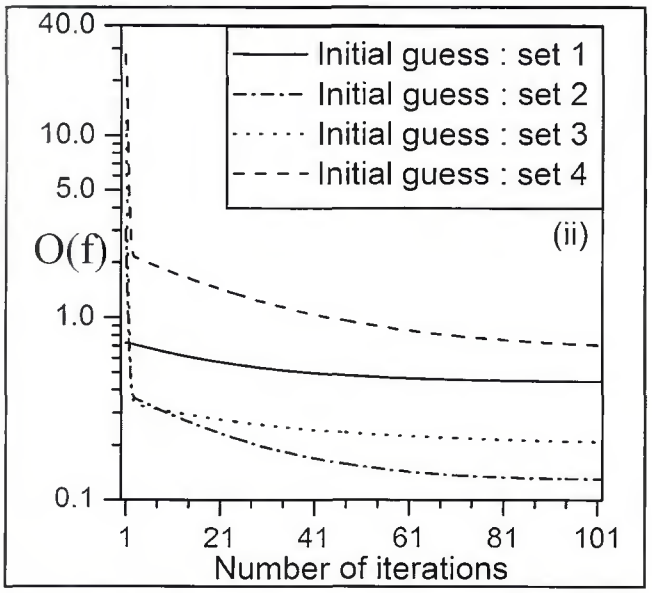


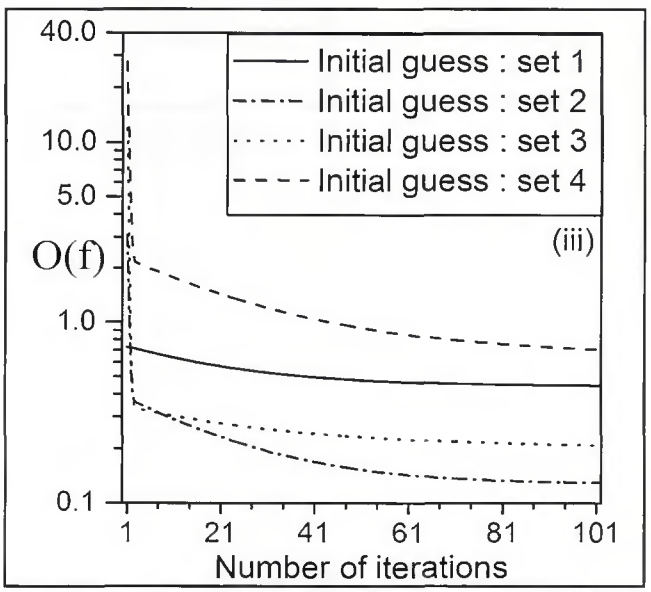


*Fig. 4 — Progress of calculation with four sets of intitial guessed values using (i) LM method, (ii) CGPR method, and (iii) CGFR method. The initial guessed values are presented in Table 6.*

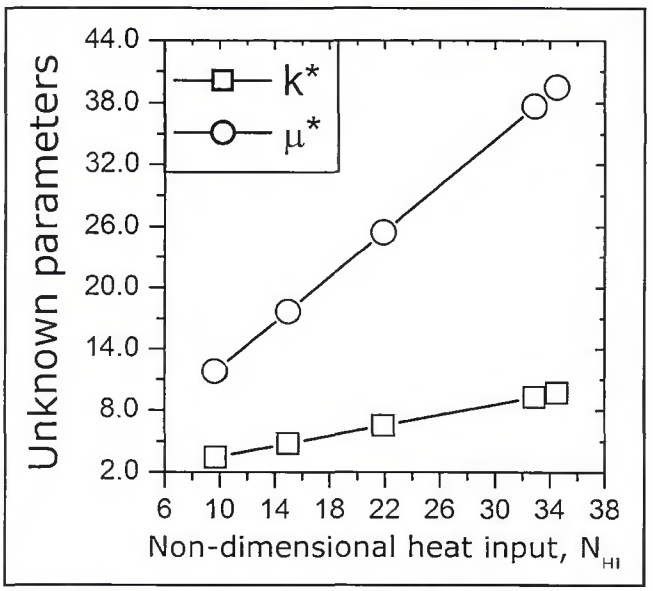


*Fig. 5 — Estimated optimum values of k* and μ* for all values of $N_{HI}$. (Optimum value of η = 0.25 for all values of $N_{HI}$)*

The total enthalpy H is represented by a sum of sensible heat h and latent heat content ΔH, i.e., H = h + ΔH where h = ≡$C_p$ dT, $C_p$ is the specific heat, T is the temperature, ΔH = $f_L$L, L is the latent heat of fusion and the liquid fraction $f_L$ is assumed to vary linearly with temperature in the mushy zone ·(Ref. 4).

$$f_L = \begin{cases} 1 & T > T_L \\ \dfrac{T - T_S}{T_L - T_S} & T_s \le T \le T_L \\ 0 & T < T_S \end{cases} \quad (5)$$

where $T_L$ and $T_S$ are the liquidus and solidus temperature, respectively. The thermal energy transport in the weld workpiece can be expressed by the following modified energy equation (Refs. 4, 21):

$$\rho\frac{\partial h}{\partial t} + \rho\frac{\partial (u_i h)}{\partial x_i} = \frac{\partial}{\partial x_i}\left(\frac{k}{C_p}\frac{\partial h}{\partial x_i}\right) - \rho\frac{\partial \Delta H}{\partial t} - \rho\frac{\partial (u_i \Delta H)}{\partial x_i} - \rho U\frac{\partial h}{\partial x_i} - \rho U\frac{\partial \Delta H}{\partial x_i} \quad (6)$$

where k is the thermal conductivity. The effective thermal conductivity in the liquid weld pool is also a property of the specific welding system and not a fundamental property of the liquid metal. Therefore, the value of the effective thermal conductivity is not known. Since the weld is symmetrical about the weld centerline only half of the workpiece is considered. The weld top surface is assumed to be flat. The velocity boundary condition is given as (Ref. 4)

$$\mu\frac{\partial u}{\partial z} = f_L\frac{d\gamma}{dT}\frac{\partial T}{\partial x}$$
$$\mu\frac{\partial v}{\partial z} = f_L\frac{d\gamma}{dT}\frac{\partial T}{\partial y}$$
$$w = 0 \quad (7)$$

where u, v, and w are the velocity components along the x, y, and z directions, re-

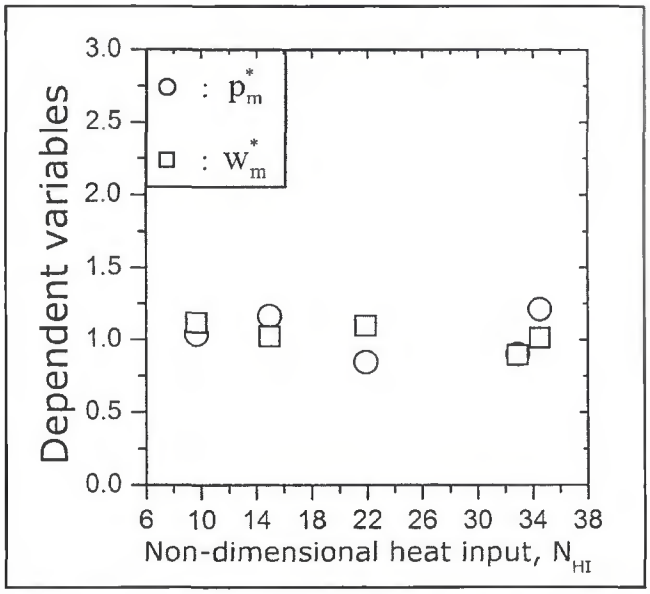


*Fig. 6 — Computed values of $p^*_m$ and $w^*_m$ using the optimized set of k* and μ* for all values of $N_{HI}$.*

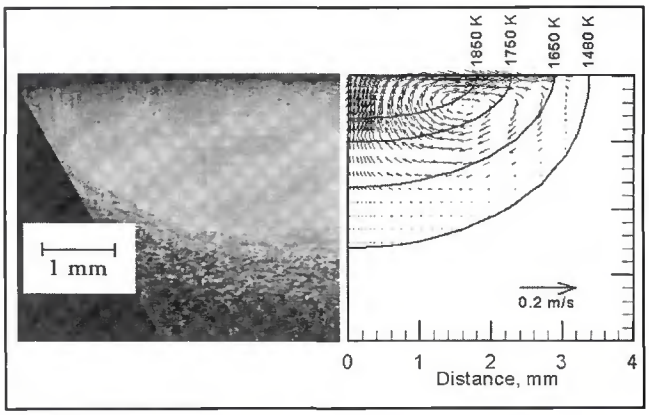


*Fig. 7 — Experimentally determined and computed weld pool geometry. The length of the black arrow shows the magnitude of the velocities and the solid lines show the isotherms. Welding parameters: P = 5000 W, η = 0.25, and v = 8.33 mm/s ($N_{HI}$ = 34.53).*

spectively, γ is the surface tension, and T is the temperature. The w velocity is zero, since the liquid metal is not transported across the weld pool top surface. The heat flux at the top surface is given as

$$k\frac{\partial T}{\partial z}=\frac{dP}{\pi r_b^2}\exp\left(-\frac{d\left(x^2+y^2\right)}{r_b^2}\right)-\left(T^4-T_a^4\right)-h_c\left(T-T_a\right) \quad (8)$$

where $r_b$ is the laser beam radius, d is the beam distribution factor, P is the laser beam power, η is the absorptivity, σ is the Stefan-Boltzmann constant, $h_c$ is the heat transfer coefficient, and $T_a$ is the ambient temperature. The first term on the RHS is the heat input from the heat source, defined by a Gaussian heat distribution. The second and third terms represent the heat loss by radiation and convection, respectively. The boundary conditions are defined as zero flux across the symmetric surface (i.e. at y = 0) as (Refs. 4, 21)

$$\frac{\partial u}{\partial y}=0,\ v=0,\ \frac{\partial w}{\partial y}=0,\ \text{and}\ \frac{\partial h}{\partial y}=0 \quad (9, 10)$$

At all other surfaces, temperatures are taken as ambient temperature and the velocities are set to zero.

## Optimization Procedure

Both the Levenberg-Marquardt (LM) and the conjugate gradient (CG) methods have been described in the literature (Refs. 39–42) and only the special features of their application are described here. The optimization of the absorptivity, effective thermal conductivity and effective viscosity begins with the construction of an objective function that depicts the difference between the computed and the measured values of weld dimensions.

### Levenberg-Marquart (LM) Method

In the LM method, the search for the optimized values follows the direction of the objective function gradient with step size modification by an adjustable damping parameter after each iteration. In the CG method, the direction of optimization is a conjunction of objective function gradient direction and the previous iteration direction (Refs. 39–42). The objective function, O(f) is defined as

$$O(f)=\sum_{m=1}^{m}\left[\frac{p_m^c-p_m^{obs}}{p_m^{obs}}\right]+\sum_{m=1}^{M}\left[\frac{w_m^c-w_m^{obs}}{w_m^{obs}}\right]=\sum_{m=1}^{M}\left[p_m^*-1\right]^2+\sum_{m=1}^{M}\left[w_m^*-1\right]^2 \quad (11)$$

where $p^c_m$ and $w^c_m$ are the penetration and the width of the weld pool computed by the numerical heat transfer and fluid flow model, respectively, $p^{obs}_m$ and $w^{obs}_m$ are the corresponding measurements at similar welding conditions and $p^*_m$ and $w^*_m$ are nondimensional and indicate the extent of over or underprediction of penetration and weld width, respectively. In Equation 11, the subscript m refers to a specific weld in a series of M number of total welds and f corresponds to the given set of three unknown parameters in nondimensional forms as

$$\{f\}\equiv\{f_1\ f_2\ f_3\}\equiv\left\{k^*\ \mu^*\ \eta\right\}\equiv\left\{\frac{k_{eff}}{k_s}\ \frac{\mu}{\mu_{fl}}\ \eta\right\} \quad (12)$$

where $k_s$, $\mu_{fl}$, $k_{eff}$, μ, and η are thermal conductivity of solid material at room temperature, viscosity of molten iron at 1823 K, effective thermal conductivity, effective viscosity of liquid metal, and absorptivity, respectively. Assuming that O(f) is continuous and has a minimum value, the LM method tries to obtain the optimum values of $f_1$, $f_2$, and $f_3$ by minimizing O(f) with respect to them. In other words, Equation 11 is differentiated with respect to $f_1$, $f_2$ and $f_3$, and each derivative is made equal to zero as

$$\left(\frac{\partial O(f)}{\partial f_i}\right)_{i=1,3}=2\left[\sum_{m=1}^{M}\left(p_m^*-1\right)\frac{\partial p_m^*}{\partial f_i}+\sum_{m=1}^{M}\left(w_m^*-1\right)\frac{\partial w_m^*}{\partial f_i}\right]_{i=1,3}=0 \quad (13)$$

where $f_i$ represents k*, μ* or, η. The variables $p^c_m$ and $w^c_m$ in Equation 13 are obtained from the numerical heat transfer and fluid flow calculations for a certain set of $f_1$, $f_2$, and $f_3$, i.e. k*, μ*, and η. The partial derivatives in Equation 13 are referred as sensitivity of the computed weld width and penetration with respect to the unknown parameters. The values of the sensitivity terms are numerically calculated. For example, the sensitivity of $p^*_m$ with respect to $f_1$ is calculated as

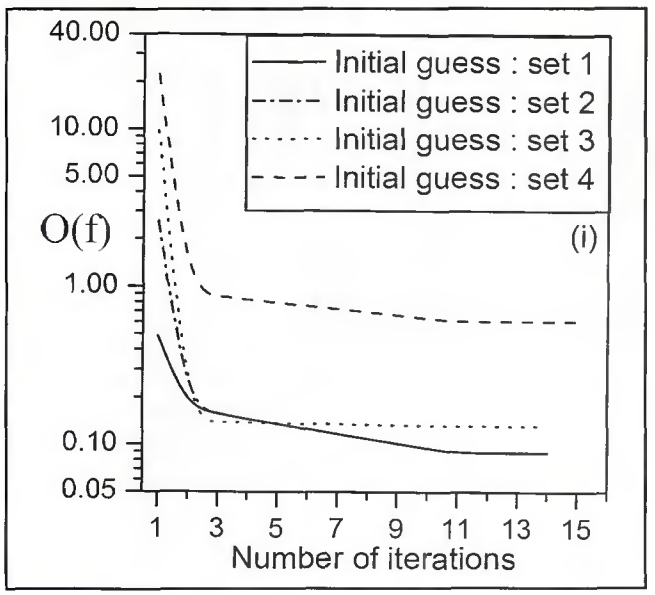


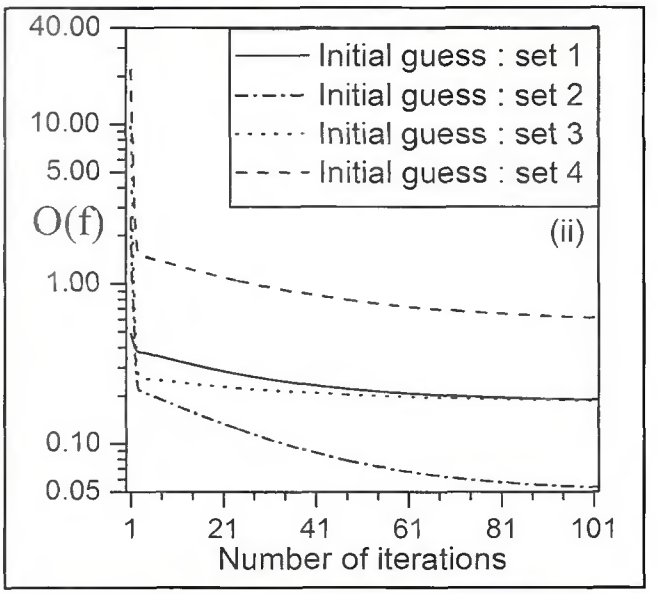


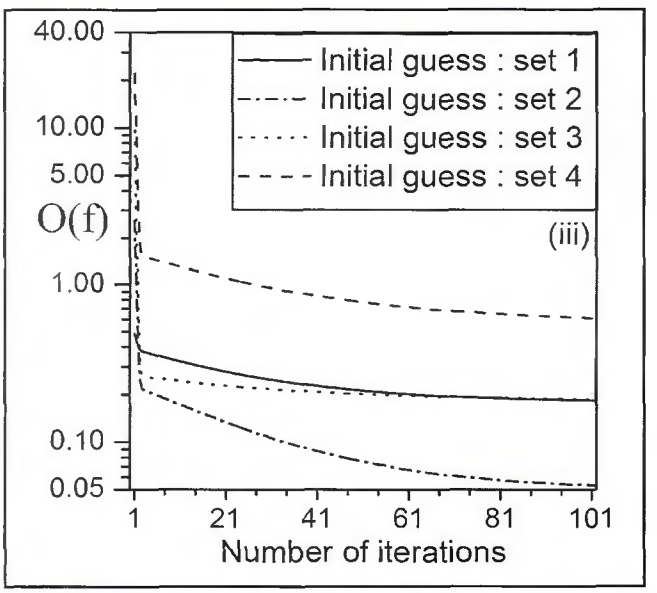


*Fig. 8 — Progress of calculation with four sets of initial guessed values using (i) LM, (ii) CGPR, and (iii) CGFR methods with three sets of measurements ($N_{HI}$ = 14.97, 32.90 and 34.53). The initial guessed values are presented in Table 6.*

$$\frac{\partial p_m^*}{\partial f_1} = \frac{p_m^*\left(\begin{matrix} f_1+\delta f_1, f_2, f_3, \\ \text{other known parameters}\end{matrix}\right) - p_m^*\left(\begin{matrix} f_1, f_2, f_3, \\ \text{other known parameters}\end{matrix}\right)}{\delta f_1} \quad (14)$$

where $\delta f_1$ is very small compared with $f_1$. The solution of Equation 13 is achieved when both $p_m^*$ and $w_m^*$ becomes close to one. In other words, the calculated values of $p_m^c$ and $w_m^c$ should be close to the corresponding measured values of $p_m^{obs}$ and $w_m^{obs}$ for all M welds. Since $f_1$, $f_2$, and $f_3$ do not explicitly appear in Equation 13, this equation needs to be rearranged so that it can serve as a basis for an iterative scheme to evaluate the optimum values of $f_1$, $f_2$, and $f_3$. The procedure is explained in Appendix 1. The final form of equations to be solved is

$$[S]\{\Delta f^k\} = -\{S^*\} \quad (15)$$

where,

$$\{f_i^{k+1}\} = \{f_i^k\} + \{\Delta f_i^k\} \text{ for } i = 1,3 \quad (16)$$

and $\{f_i^{k+1}\}$ refers to the three unknown increments after $(k+1)^{th}$ iteration. Equation 15 provides the solution of the three unknown increments, $\{\Delta f_i^k\}$ corresponding to the three unknown parameters.

### Conjugate Gradient (CG) Method

In the conjugate gradient technique, the unknown parameters are iteratively searched in the following sequence (Refs. 40–42):

$$f_i^{k+1} = f_i^k - \beta^k d_i^k \text{ for } i = 1,3 \quad (17)$$

where $f_i^{k+1}$ represents the values of the three unknowns after $(k+1)^{th}$ iteration, indicates the directions of search at the end of $k^{th}$ iteration corresponding to the unknowns $f_1$, $f_2$, and $f_3$, and $\beta^k$ is the size of the search step. Both $d_i^k$ and $\beta^k$ are calculated for every iteration or step. The variable $\beta^k$ tends to adjust the extent of increment in unknown parameters between successive iterations and logically should assume a value that will facilitate the condition of objective function minimum. Thus, $\beta^k$ is calculated by minimizing the residual objective function $O(f_i)^{k+1}$

$$\frac{\partial O(f_i)^{k+1}}{\partial \beta^k} = 0 \; ; \; \beta^k \geq 0 \quad (18)$$

The directions of search, $d_1^k$, $d_2^k$, and $d_3^k$, at the end of $k^{th}$ iteration are calculated as a linear conjugation of the corresponding directions of search at the end of $(k-1)^{th}$ iteration and the respective residual gradient of the objective function, O(f), after $k^{th}$ iteration as

$$\begin{aligned} d_1^k &= \nabla O\left(f_1^k\right) + \gamma^k d_1^{k-1} \\ d_2^k &= \nabla O\left(f_2^k\right) + \gamma^k d_2^{k-1} \\ d_3^k &= \nabla O\left(f_3^k\right) + \gamma^k d_3^{k-1} \end{aligned} \quad (19)$$

where $\gamma^k$ is a conjugation coefficient at the end of $k^{th}$ iteration. The coefficient $\gamma^k$ is obtained either by Equation 20a using Polok-Ribier's (CGPR) modification or by Equation 20b using Fletcher-Reeve's modification (CGFR)

$$\gamma^k = \frac{\sum_{i=1}^{3}\left\{\nabla O\left(f_i^k\right)\right\}^2}{\sum_{i=1}^{3}\left\{\nabla O\left(f_i^{k-1}\right)\right\}^2}$$

$$\text{for } k = 1,2,\ldots \text{ and } \gamma^0 = 0 \quad (20a)$$

$$\gamma^k = \frac{\sum_{i=1}^{3}\left\{\nabla O\left(f_i^k\right)\right\}\left\{\nabla O\left(f_i^k\right) - \nabla O\left(f_i^{k-1}\right)\right\}}{\sum_{i=1}^{3}\left\{\nabla O\left(f_i^{k-1}\right)\right\}^2}$$

$$\text{for } k = 1,2,\ldots \text{ and } \gamma^0 = 0 \quad (20b)$$

**Table 5 — Data Used for Calculations of Temperature and Vetocity Fields[a]**

| Physical Property | Value |
|---|---|
| Liquidus temperature, $T_L$ (K) | 1800.0 |
| Solidus temperature, $T_S$ (K) | 1760.0 |
| Ambient temperature, $T_a$ (K) | 293.0 |
| Density of liquid metal, $\rho$ (kg/m$^3$) | $7.2 \times 10^3$ |
| Thermal conductivity of solid, $k_s$ (W m$^{-1}$ K$^{-1}$) | 25.08 |
| Thermal conductivity of liquid, $k_L$ (W m$^{-1}$ K$^{-1}$) | 25.08 |
| Specific heat of solid, $C_{PS}$ (J kg$^{-1}$ K$^{-1}$) | 754.0 |
| Specific heat of liquid, $C_{PL}$ (J kg$^{-1}$ K$^{-1}$) | 754.0 |
| Temperature coefficient of surface tension, d$\gamma$/dT (N m$^{-1}$ K$^{-1}$) | $-0.5 \times 10^{-3}$ |
| Coefficient of thermal expansion, $\beta$ (K$^{-1}$) | $1.5 \times 10^{-6}$ |
| Viscosity of molten iron at 1823 K, $\mu_{fl}$ (kg.m$^{-1}$s$^{-1}$) | $6.7 \times 10^{-3}$ |

(a) for data set index 3 and 4 (Ref. 24).

**Table 6 — Sets of Initial Guesses for the Unknown parameters, $C_2$ and $C_4$**

| Set 1 | Set 2 | Set 3 | Set 4 | Optimized values |
|---|---|---|---|---|
| $C_2 = 0.5$ | $C_2 = 1.0$ | $C_2 = 1.5$ | $C_2 = 2.0$ | $C_2 = 0.252$ |
| $C_4 = 0.5$ | $C_4 = 1.0$ | $C_2 = 1.5$ | $C_4 = 2.0$ | $C_4 = 1.115$ |
| $\eta = 0.1$ | $\eta = 0.2$ | $\eta = 0.3$ | $\eta = 0.4$ | $\eta = 0.250$ |

Further details of these two approaches are given in Appendix 2. In the CG methods, the direction of search is important, since the solution may diverge if the direction of search loses sight of the optimal solution. In the LM method, a manual damping factor is used that continually tracks the search step (or increment) so that the optimal solution cannot move away from the last computed minimum value of the objective function.

There are two main limitations in finding property data by the coupled heat and fluid flow and optimization procedure described in this manuscript. They are 1) the accuracy of measured depth and width and 2) how strongly the depth and the width vary with the uncertain parameter (sensitivity).

## Results and Discussion

The sensitivity of the computed weld pool dimensions with respect to the effective thermal conductivity, effective viscosity, and absorptivity were determined by several heat transfer and fluid flow calculations. Figures 1A and B depict a number of isocontours of the dimensionless penetration, $p^*_m$, and the dimensionless width, $w^*_m$, as a function of $k^*$ and $\mu^*$ for data set No. 3 in Table 1. It is observed from Fig. 1A that the dimensionless penetration, $p^*_m$, increases with $k^*$ or $\mu^*$. However, the dimensionless width, $w^*_m$, decreases with $k^*$ or $\mu^*$ as shown in Fig. 1B. For $k^*$ values above 7.0, both $p^*_m$ and $w^*_m$ become fairly insensitive to $\mu^*$. Furthermore, both $p^*_m$ and $w^*_m$ approached a value of unity at high values of $k^*$ and $\mu^*$. When both $p^*_m$ and $w^*_m$ are 1, $p^c_m$ equals $p^{obs}_m$ and $w^c_m$ equals $w^{obs}_m$ and the calculated results agree with the corresponding measured values.

The effects of $k^*$ and $\mu^*$ on the computed weld pool dimensions can be explained as follows:

The dimensionless weld penetration, $p^*_m$, increases with $k^*$ since high values of thermal conductivity facilitate rapid heat transport in the downward direction. However, the higher thermal conductivity also reduces the surface temperature gradient and the radial convective heat transport and, consequently, decreases. Higher values of $\mu^*$ lowers radial convection and the convective heat flow resulting in both lower weld width and slightly higher peak temperature. The higher peak temperature enhances downward heat conduction and increases penetration. Furthermore, as $k^*$ is progressively increased, conduction becomes the dominant mechanism of heat transfer and changes in $\mu^*$ do not significantly alter either the peak temperature or the convective heat transfer rate. Thus, the weld pool dimensions do not change significantly with $\mu^*$ at high values of $k^*$ as observed in Fig. 1A and B.

It is quite apparent that in addition to the variation in $k^*$ or $\mu^*$, any change in the value of absorptivity will further influence the results presented in Fig. 1A and B. Although it has been reported that $\eta$ depends on laser power (Ref. 43), the absorptivity is a material property, and its exact value depends on factors such as the surface temperature. An increase in the value of absorptivity implies an enhancement in the heat absorption rate that leads to higher peak temperature, greater temperature gradient and larger computed weld pool dimensions for a specific set of $k^*$ and $\mu^*$. In contrast, a decrease in the value of absorptivity leads to smaller values of computed weld pool dimensions for a specific set of $k^*$ and $\mu^*$. Such a behavior was also demonstrated in the case of a GTA weld pool (Ref. 29). To keep the problem tractable, a single optimized value of absorptivity ($\eta$) for all the welding conditions considered in the present work is assumed.

Figure 2 shows that high values of $k^*$ and $\mu^*$ are necessary to achieve good agreement between the computed and the experimental weld pool geometry, i.e., low values of objective function for data set No. 3 in Table 1. In contrast, Fig. 3 indicates that low values of both $k^*$ and $\mu^*$ are necessary to reduce the objective function for data set No. 2 in Table 1. These apparently contrasting results are achieved for welds with different heat input indexes ($N_{HI}$) of 21.90 and 14.97 for data set Nos. 3 and 2, respectively. The results in Figs. 2 and 3 are consistent with the fact that $k^*$ and $\mu^*$ are not materials properties and their optimum values depend on $N_{HI}$. To account for the same in the procedure of optimization of $k^*$ and $\mu^*$ in a simplified manner, the following linear relationships are assumed for simplicity:

$$k^* = C_1 + C_2 N_{HI}$$
$$\mu^* = C_3 + C_4 N_{HI} \qquad (21)$$

where $C_1$ and $C_3$ are the minimum values of the effective conductivity and effective viscosity, respectively, and $C_2$, and $C_4$ are constants. Since $k^*$ and $\mu^*$ equal 1 at low values of $N_{HI}$, the values of both $C_1$ and $C_3$ are taken to be one. Thus, the optimization routine is used to estimate the values of $C_2$ and $C_4$ for each $N_{HI}$.

Results in Figs. 2 and 3 also indicate that several combinations of $k^*$ and $\mu^*$ may result in low values of O(f) for a given $N_{HI}$. In order to seek optimum values for $k^*$ and $\mu^*$ for a particular $N_{HI}$, an additional constraint is useful to achieve a physically realistic solution. Since $k^*$ and $\mu^*$ are related by the turbulent Prandtl number, $Pr_T$, its value (= 0.9) provides a useful constraint. In other words, out of many possible solutions, the specific combination of $k^*$ and $\mu^*$ nearest to the line corresponding to $Pr_T$ = 0.9 will be chosen as the final solution. $Pr_T$ is defined as

$$Pr_T = \frac{\mu_T C_{PL}}{k_T} \qquad (22)$$

where $\mu_{eff} = \mu_L + \mu_T$, $k_{eff} = k_L + k_T$ and $\mu_T$, $k_T$ are the turbulent viscosity and thermal conductivity, respectively, and $\mu_L$ and $k_L$ are the viscosity and thermal conductivity of the liquid, respectively. Finally, Equation 12 is modified as

$$\{f\} \equiv \{f_1 f_2 f_3\} \equiv \{C_2\ C_4\ \eta\} \qquad (23)$$

A set of initial values of $C_2$, $C_4$ and $\eta$ is necessary to start the optimization calculations by all three methods indicated in Appendixes 1 and 2. It is apparent from

Figs, 1 through 3 that the expression $(\partial O(f)/\partial f_{i=t,3}$ does not conform to a continuous, convex, or concave-type function and the solution of Equation 13 involves multiple local minima in the objective function. To address this difficulty, the optimization calculations have been performed with a number of initial values in the ranges of 0.10 to 3.0, 0.10 to 3.0, and 0.10 to 0.50 for $C_2$, $C_4$, and $\eta$, respectively. Table 6 presents four such representative sets of initial values for which the progress of the optimization calculations are presented in Figures 4(i) to (iii). All measured weld pool dimensions indicated in Table 1 were used for the optimization. These figures show that the minimum attainable value of O(f) is affected by the choice of the initial values in both LM and CG methods. In the LM method, the minimum value of O(f) was obtained when the 1st and 2nd set of initial values (Table 6) were used (Fig. 4i) while the 3rd and 4th set of initial values resulted in values of O(f) as 0.219 and 0.837, respectively. In both the CGPR and CGFR methods, a minimum value of O(f) = 0.129 was achieved when the 2nd set of initial values (Table 6) were used (Figs. 4ii and 4iii). The value of O(f) could not be reduced below 0.129 with various other sets of initial guesses using all three optimization procedures. The final optimum solutions of $C_2$, $C_4$ and $\eta$ corresponding to O(f) = 0.129 were the same regardless of the initial guessed values of $C_2$, $C_4$ and $\eta$. For example, a set of initial values of $C_2$, $C_4$ and $\eta$ equal to 1.0, 1.0, and 0.3, respectively, yielded nearly similar values of O(f) and the optimized solution of $C_2$, $C_4$ and $\eta$ were the same as those obtained with the 2nd set of initial values (Table 6). Although a reduction in the value of O(f) from 0.166 in the LM method to 0.129 in the CG method appears to be small, it should be noted that O(f) depicts the square of the summation of the actual errors representing the discrepancy between $p_m^c$ and $p_m^{obs}$, and $w_m^c$ and $w_m^{obs}$. This discrepancy can be important even for small values of O(f) and achieving the smallest possible value of O(f) is important.

A closed-form relationship between the dependent variables such as the weld dimensions and the unknown parameters does not exist. As a result, the lowest value of O(f) depends on the initial guessed values of the unknown parameters. At the start of the iterations, the initial few gradients of the objective function with respect to the unknown parameters affect the results of the subsequent iterations and, ultimately, the optimum value of O(f). One way to resolve the difficulty resulting from the absence of a closed-form relation between the objective function and the unknown parameters is to perform the optimization with a number of initial values so as to arrive at a best possible optimum solution. Furthermore, the optimization in the present work was computationally intensive, since the number of numerical heat transfer and fluid flow calculations for each optimization iteration was equal to the number of variables multiplied by the number of welds for sensitivity calculation plus the number of welds for error verification. However, an appropriate choice of the initial values could significantly reduce the volume of the computational work. Based on the results of optimization, Equation (21) can be rewritten as

$$k^* = 1.0 + 0.252\, N_{HI}$$

$$\mu^* = 1.0 + 1.115\, N_{HI} \qquad (24)$$

The effectiveness of the optimization process is evident from the fact that all three optimization methods resulted in nearly similar sets of the optimum values of $C_2$, $C_4$, and $\eta$.

Figure 5 shows that both $k^*$ and $\mu^*$ increase significantly with $N_{HI}$ consistent with Equation 24. This behavior is expected since higher heat input leads to more rapid transport of momentum and heat. The computed values of $p_m^*$ and $w_m^*$ using the optimized values of $k^*$ and $\mu^*$ are plotted in Fig. 6 for all values of $N_{HI}$. A fairly satisfactory agreement is obtained between the computed and measured weld dimensions. The slight discrepancy between the computed and the experimental values can be attributed, at least in part, to the experimental errors.

Typical computed temperature and velocity fields are shown in Fig. 7. The results show that the liquid metal is transported from the middle of the pool outward due to a negative temperature coefficient of surface tension. The features of the computed temperature and velocity fields are typical of the Marangoni convection dominated laser melted pools and have been discussed in the literature (Refs. 16, 19, 20, 24, 26, 27).

A test for the effectiveness of the proposed deterministic model is to check if the values of the uncertain parameters can be evaluated from a relatively small volume of experimental data. For this purpose, the values of $C_2$, $C_4$, and $\eta$ were determined from the experimental data for three welds with $N_{HI}$ = 14.97, 32.90, and 34.53 in Table 1. Figures 8(i) through (iii) show the variation of the objective function with number of iterations for four sets of initial guesses presented in Table 6 using all three optimization methods. It is observed that the LM method can provide an approximate minimum value of O(f) ⊕0.089 when the 1st and 2nd set of initial values (Table 6) are used — Fig. 8i. Both CGPR and CGFR routines could reach the minimum values of O(f) only when the 2nd set of initial values (Table 6) is used — Figs. 8ii and 8iii. The minimum value of O(f) could be reached within ten iterations using the LM routine and around 80 iterations in both CGPR and CGFR methods. The values of $C_2$, $C_4$, and $\eta$ were found to be 0.252, 1.115, and 0.253, respectively, corresponding to the minimum value of O(f) following CG methods. Following the LM method, the optimized values of $C_2$, $C_4$, and $\eta$ were found to be 0.265, 1.138, and 0.228, respectively, when only three sets of experimental data were used in the optimization process. The optimized values of these parameters did not change significantly when all five sets of experimental data were used for optimization.

The values of $k^*$ and $\mu^*$ estimated in the present work are within the range of enhancement factors reported in the literature. For example, values in the range of 30 to 100 for both $k^*$ and $\mu^*$ were estimated through trial and error to achieve good agreement between the computed and the measured weld dimensions (Ref. 27). When the k-ε turbulence model with a spatially variable effective viscosity was used, a maximum value of 16 for $\mu^*$ was reported for a stationary GTA weld pool (Ref. 26). Although the value of $\eta$ and the relationships between $N_{HI}$ and $k^*$, and $\mu^*$ are valid for the specific conditions of welding considered here, a similar approach can be adopted for other welding conditions (Refs. 29, 30). Since $\eta$, $k^*$ and $\mu^*$ are linked with $p_m^*$ and $w_m^*$ through the equations of conservation of mass, momentum and energy rather than through a straightforward polynomial function, local minima should be avoided by repeating the procedure with several sets of initial values. The intensive computational work needed to determine the uncertain parameters results in enhanced reliability of the numerical modeling of heat transfer and fluid flow in the weld pool.

## Summary and Conclusions

Reliability of numerical heat transfer and fluid flow calculations in the weld pool can be significantly enhanced by determining the optimized values of effective thermal conductivity, effective viscosity, and absorptivity from a limited volume of measured weld dimensions. Three versions of gradient-based optimization techniques could produce low values of an objective function and determine the three aforementioned parameters. Although the values of these parameters were independent of the optimization process, the volume of the calculations needed and the manner in which the optimized values were obtained depended on both the opti-

mization method selected and the initial guessed values of the parameters. The values of effective thermal conductivity and effective viscosity were found to be much higher than their corresponding molecular values and also depended on heat input. Correlations are proposed to determine these parameters from welding conditions. The use of the optimized values of absorptivity, effective thermal conductivity and effective viscosity, determined from a limited volume of experimental data and the proposed model, resulted in good agreement between the computed and the experimentally determined fusion zone geometry without the need to adjust these parameters by trial and error.

*Acknowledgments*

The work was supported by a grant from the U.S. Department of Energy, Office of Basic Energy Sciences, Division of Materials Sciences, under grant number DE-FGO2-01ER45900. The authors appreciate critical comments on the work from Mr. S. Mishra, Ms. Xiuli He and Mr. A. Kumar.

*References*

1. David, S. A., and DebRoy, T. 1992. Current issues and problems in welding science. *Science* 257: 497–502.

2. DebRoy, T., and David, S. A. 1995. Physical processes in fusion welding. *Rev. Mod. Phys.* 67(1): 85–112.

3. Zhao, H., White, D. R., and DebRoy, T. 1999. Current issues and problems in laser welding of aluminum alloys. *Int. Mater. Rev.* 44: 238–266.

4. Mundra, K., DebRoy, T., and Kelkar, K. M. 1996. Numerical prediction of fluid flow and heat transfer in welding with a moving heat source. *Numer. Heat Transfer* A 29: 115–129.

5. Elmer, J. W., Palmer T. A., Zhang W., Wood, B., and DebRoy, T. 2003. Kinetic modeling of phase transformations occurring in the HAZ of C-Mn steel welds based on direct observations. *Acta Materialia*. 51(12): 3333–3349.

6. Kou, S., and Wang, Y. H. 1986. Three dimensional convection in laser melted pools. *Metallurgical Transactions A*. 17A(12): 2265–2270.

7. Pitscheneder, W., DebRoy, T., Mundra, K., and Ebner, R. 1996. Role of sulfur and processing variables on the temporal evolution of weld pool geometry during multi-kilowatt laser welding of steels. *Welding Journal* 75(3): 71-s to 80-s.

8. Cool, T., and Bhadeshia, H. K. D. H. 1997. Austenite formation in 9Cr1Mo type power plant steels. *Sci. Technol. Weld. Joining*. 2(1): 36–42.

9. Mishra, S., and DebRoy, T. 2004. Grain topology in Ti-6Al-4V welds — Monte Carlo simulation and experiments. *Journal of Physics D: Applied Physics*. 37: 2191–2196.

10. Mishra, S., and DebRoy, T. 2004. Measurements and Monte Carlo simulation of grain structure in the heat-affected zone of Ti-6Al-4V welds. *Acta Materialia*. 52(5): 1183–1192.

11. Yang, Z. and DebRoy, T. 1999. Modeling of macro- and microstructures of gas metal arc welded HSLA-100 steel. *Metall. Mater. Trans*. B. 30B: 483–493.

12. Hong, T., Pitscheneder, W., and DebRoy, T. 1998. Quantitative modeling of inclusion growth in the weld pool by considering their motion and temperature gyrations. *Sci. Technol. Weld. Joining*. 3(1): 33–41.

13. Hong, T., and DebRoy, T. 2003. Non-isothermal growth and dissolution of inclusions in liquid steels. *Metal. Mater. Trans*. B. 34B: 267–269.

14. Hong, T., and DebRoy, T. 2001. Effects of time, temperature and steel composition on the growth and dissolution of inclusions in liquid steels. *Ironmaking and Steelmaking*. 28(6): 450–454.

15. He, X., Fuerschbach, P., and DebRoy, T. 2004. Composition change of stainless steel during micro-joining with short laser pulse. *J. Appl. Phys*. (In press).

16. Zhao, H., and DebRoy, T. 2001. Weld metal composition change during conduction model laser welding of 5182 aluminum alloy. *Metall. Mater. Trans*. B. 32B: 163–172.

17. Palmer, T. A., and DebRoy, T. 2000. Numerical modelling of enhanced nitrogen dissolution during GTA welding. *Metall. Mater. Trans*. B. 31B(6): 1371–1385.

18. Mundra, K., Blackburn, J. M., and DebRoy, T. 1997. Absorption and transport of hydrogen during GMA welding of mild steels. *Sci. Technol. Weld. Joining*. 2(4): 174–184.

19. He, X., Fuerschbach, P. W., and DebRoy, T. 2003. Heat transfer and fluid flow during laser spot welding of 304 stainless steel. *J. Phys. D: Appl. Phys*. 36(12): 1388–1398.

20. Zhao, H. and DebRoy, T. 2003. Macroporosity free aluminum alloy weldments through numerical simulation of keyhole mode laser welding. *J. Appl. Phys*. 93(12): 10089–10096.

21. Zhang, W., Roy, G. G., Elmer, J. W., and DebRoy, T. 2003. Modeling of heat transfer and fluid flow during gas tungsten arc spot welding of low carbon steel. *J. Appl. Phys*. 93(5): 3022–3033.

22. Kumar, A., and DebRoy, T. 2003. Calculation of three-dimensional electromagnetic force field during arc welding. *J. Appl. Phys*. 94(2): 1267–1277.

23. Kim, C. H., Zhang, W. and DebRoy, T. 2003. Modeling of temperature field and solidified surface profile during gas metal arc fillet welding. *J. Appl. Phys*. 94(4): 2667–2679.

24. Pitscheneder, W. 2001. Contribution to the understanding and optimization of laser surface alloying. PhD Dissertation. University of Leoben, Austria.

25. DebRoy, T., Mazumdar, A. K., and Spalding, D. B. 1978. Numerical prediction of recirculating flows with free convection encountered in gas-stirred reactors. *Applied Mathematical Modelling*. 2: 146–150.

26. Hong, K., Weckmann, D. C., Strong, A. B., and Zheng, W. 2002. Modelling turbulent thermofluid flow in stationary gas tungsten arc welded pools. *Sci. Technol. Weld. Joining*. 7(3): 125–136.

27. Choo, R. T. C., and Szekely, J. 1994. The possible role of turbulence in GTA weld pool behavior. *Welding Journal* 73(2): 25-s to 31-s.

28. Jonsson, P. G., Szekely, J., Choo, R. T. C., and Quinn, T. P. 1994. Mathematical models of transport phenomena associated with arc welding processes: a survey. *Modelling Simul. Mater. Sci. Eng*. 2(5): 995–1016.

29. De, A., and DebRoy, T. 2004. Probing unknown welding parameters from convective heat transfer calculation and multivariate optimization. *J. Phys. D: Appl. Phys*. 37(1): 140–150.

30. De, A., and DebRoy, T. 2004. A smart model to estimate effective thermal conductivity and viscosity in weld pool. *Journal of Applied Physics*. 95(9): 5230–5240.

31. Hsu, Y. F., Rubinsky, B. and Mahin, K. 1986. An inverse finite element method for the analysis of stationary arc welding process. *J. Heat Transfer*, Trans. ASME. 108(4): 734–741.

32. Beck, J. V. 1991. Inverse problems in heat transfer with application to solidification and welding. *Proc. 5th Int. Conf. on Modeling of Casting, Welding and Advanced Solidification Processes*, eds. M. Rappaz et al., pp. 503–514. The Minerals, Metals and Materials Society, Warrendale, Pa.

33. Rappaz, M., Desbiolles, J. L., Drezet, J. M., Gandin, C. A., Jacot, A., and Thevoz, P. 1995. Proc. 7th Int. Conf. on Modeling of Casting, *Welding and Advanced Solidification Processes*, eds. M. Cross et al., pp. 449–457, The Minerals, Metals and Materials Society, Warrendale, Pa.

34. Fonda, R. W. and Lambrakos, S. G. 2002. Analysis of friction stir welds using an inverse problem approach. *Sci. Technol. Weld. Joining* 7(3): 177–181.

35. Karkhin, V. A., Plochikhine, V. V., and Bergmann, H. W. 2002. Solution of inverse heat conduction problem for determining heat input, weld shape, and grain structure during laser welding. *Sci. Technol. Weld. Joining* 7(4): 224–231.

36. Patankar, S. V. 1992. *Numerical Heat Transfer and Fluid Flow*. New York, McGraw-Hill.

37. Voller, V. R., and Prakash, C. 1987. A fixed grid numerical modeling methodology for convection-diffusion mushy region phase change problems. *Int. J. Heat Mass Transf.* 30: 1709–1719.

38. Brent, A. D., Voller, V. R., and Reid, K. J. 1988. The enthalpy porosity technique for modeling convection-diffusion phase change: application to the melting of a pure metal. *Numerical Heat Transfer* 13: 297–318.

39. Beck, J. V., and Arnold, K. J. 1977. *Parameter Estimation in Engineering and Science*. New York, N.Y., Wiley International.

40. Beck, J. V., Blackwell, B., and Clair, C. R., Jr. 1985. *Inverse Heat Conduction—Ill Posed Problems*. New York, N.Y., Wiley International.

41. Alifanov, O. M. 1994. *Inverse heat Transfer Problems*. Berlin, Springer-Verlag.

42. Ozisik, M. N., and Orlande, H. R. B. 2000. *Inverse Heat Transfer*. 35, New York, N.Y., Taylor & Francis Inc.

43. Fuerschbach, P. W. 1996. Measurement and prediction of energy transfer efficiency in laser beam welding. *Welding Journal* 75(1): 24-s to 34-s.

## Appendix 1

In order to explain the basic concept of the LM method, a simplified system involving three unknown parameters, $f_1$, $f_2$, and $f_3$, and one dependent variable, $p^*_m$ measured under five welding conditions is considered first. Equation 13 can be written for $f_1$, $f_2$, and $f_3$ as:

$$\sum_{m=1}^{5}\left[\left(p_m^*-1\right)\frac{\partial p_m^*}{\partial f_1}\right]=0;$$

$$\sum_{m=1}^{5}\left[\left(p_m^*-1\right)\frac{\partial p_m^*}{\partial f_2}\right]=0;$$

$$\sum_{m=1}^{5}\left[\left(p_m^*-1\right)\frac{\partial p_m^*}{\partial f_3}\right]=0$$

(A1, A2, A3)

The values of the three unknowns, $f_1$, $f_2$, and $f_3$ cannot be directly obtained from the above equations since they do not appear explicitly in these equations. The symbols $f_1$, $f_2$, and $f_3$ resemble $k^*$, $\mu^*$, and $\eta$ (absorptivity), respectively. So, the dependent variable $p_m^*$ is expanded using the Taylor's series expansion to explicitly contain values of increments and, $f_1$, $f_2$, and $f_3$. Considering two successive iterations of $p^*_m$ and taking only the first order terms

$$\left(p_m^*\right)^{k+1}=\left(p_m^*\right)^k+\frac{\partial\left(p_m^*\right)^k}{\partial f_1}\Delta f_1^k+\frac{\partial\left(p_m^*\right)^k}{\partial f_2}\Delta f_2^k+\frac{\partial\left(p_m^*\right)^k}{\partial f_3}\Delta f_3^k \quad \text{(A4)}$$

where $\Delta f_1^k$, $\Delta f_2^k$ and $\Delta f_3^k$ are three unknown increments corresponding to $f_1$, $f_2$, and $f_3$ as

$$f_1^{k+1}=f_1^k+\Delta f_1^k$$
$$f_2^{k+1}=f_2^k+\Delta f_2^k$$
$$f_3^{k+1}=f_3^k+\Delta f_3^k \quad \text{(A5)}$$

and $f_1^{k+1}$, $f_2^{k+1}$, and $f_3^{k+1}$ correspond to the values of three unknowns after $(k+1)^{th}$ iteration. Except $\Delta f_1^k$, $\Delta f_2^k$, and $\Delta f_3^k$, all other terms on the right hand side of Equation A4 are considered to be known. To solve for $\Delta f_1^k$, $\Delta f_2^k$, and $\Delta f_3^k$, Equations A1, A2 and A3 are first rewritten replacing $p_m^*$ by $(p_m^*)^{k+1}$ as

$$\sum_{m=1}^{5}\left[\left(\left(p_m^*\right)^{k+1}-1\right)\frac{\left(\partial p_m^*\right)^{k+1}}{\partial f_1}\right]=0;$$

$$\sum_{m=1}^{5}\left[\left(\left(p_m^*\right)^{k+1}-1\right)\frac{\left(\partial p_m^*\right)^{k+1}}{\partial f_2}\right]=0$$

$$\sum_{m=1}^{5}\left[\left(\left(p_m^*\right)^{k+1}-1\right)\frac{\left(\partial p_m^*\right)^{k+1}}{\partial f_3}\right]=0$$

(A6, A7, A8)

However, $p_m^*$ equals to $p_m^c/p_m^{obs}$, and although $p_m^{obs}$ is a known measured value, $p_m^c$ is to be computed using the numerical heat transfer and fluid flow calculation for a set of $f_1$, $f_2$, $f_3$ and other known parameters. So, $(p_m^*)^{k+1}$ that is the value of $p_m^*$ after $(k+1)^{th}$ iteration is unknown since $\Delta f_1^k$, $\Delta f_2^k$,and $\Delta f_3^k$ are unknown. Next, substituting right hand side of Equation A4 in the place of $(p_m^*)^{k+1}$, Equations A6, A7, and A8 are rewritten as:

$$\sum_{m=1}^{5}\left[\frac{\partial\left(\begin{array}{l}\left(p_m^*\right)^k+\dfrac{\partial\left(p_m^*\right)^k}{\partial f_1}\Delta f_1^k+\\ \dfrac{\partial\left(p_m^*\right)^k}{\partial f_2}\Delta f_2^k+\dfrac{\partial\left(p_m^*\right)^k}{\partial f_3}\Delta f_3^k-1\end{array}\right)}{\partial f_1}\left(\begin{array}{l}\left(p_{m*}\right)^k+\dfrac{\partial\left(p_m^*\right)^k}{\partial f_1}\Delta f_1^k+\\ \dfrac{\partial\left(p_m^*\right)^k}{\partial f_2}\Delta f_2^k+\dfrac{\partial\left(p_m^*\right)^k}{\partial f_3}\Delta f_3^k\end{array}\right)\right]=0 \quad \text{(A9)}$$

$$\sum_{m=1}^{5}\left[\frac{\partial\left(\begin{array}{l}\left(p_m^*\right)^k+\dfrac{\partial\left(p_m^*\right)^k}{\partial f_1}\Delta f_1^k+\\ \dfrac{\partial\left(p_m^*\right)^k}{\partial f_2}\Delta f_2^k+\dfrac{\partial\left(p_m^*\right)^k}{\partial f_3}\Delta f_3^k-1\end{array}\right)}{\partial f_2}\left(\begin{array}{l}\left(p_{m*}\right)^k+\dfrac{\partial\left(p_m^*\right)^k}{\partial f_1}\Delta f_1^k+\\ \dfrac{\partial\left(p_m^*\right)^k}{\partial f_2}\Delta f_2^k+\dfrac{\partial\left(p_m^*\right)^k}{\partial f_3}\Delta f_3^k\end{array}\right)\right]=0 \quad \text{(A10)}$$

$$\sum_{m=1}^{5}\left[\frac{\partial\left(\begin{array}{l}\left(p_m^*\right)^k+\dfrac{\partial\left(p_m^*\right)^k}{\partial f_1}\Delta f_1^k+\\ \dfrac{\partial\left(p_m^*\right)^k}{\partial f_2}\Delta f_2^k+\dfrac{\partial\left(p_m^*\right)^k}{\partial f_3}\Delta f_3^k-1\end{array}\right)}{\partial f_3}\left(\begin{array}{l}\left(p_{m*}\right)^k+\dfrac{\partial\left(p_m^*\right)^k}{\partial f_1}\Delta f_1^k+\\ \dfrac{\partial\left(p_m^*\right)^k}{\partial f_2}\Delta f_2^k+\dfrac{\partial\left(p_m^*\right)^k}{\partial f_3}\Delta f_3^k\end{array}\right)\right]=0 \quad \text{(A11)}$$

Neglecting higher order differentials e.g

$$\frac{\partial}{\partial f_1}\left(\frac{\partial\left(p_m^*\right)}{\partial f_1}\Delta f_1^k\right)$$ etc., Equations A9, A10 and A11 are further simplified as:

$$\sum_{m=1}^{5}\left[\left(\begin{array}{l}\left(p_m^*\right)^k+\dfrac{\partial\left(p_m^*\right)^k}{\partial f_1}\Delta f_1^k+\\ \dfrac{\partial\left(p_m^*\right)^k}{\partial f_2}\Delta f_2^k+\\ \dfrac{\partial\left(p_m^*\right)^k}{\partial f_3}\Delta f_3^k-1\end{array}\right)\frac{\partial\left(p_m^*\right)^k}{\partial f_1}\right]=0 \quad \text{(A12)}$$

$$\sum_{m=1}^{5}\left[\left(\begin{array}{l}\left(p_m^*\right)^k+\dfrac{\partial\left(p_m^*\right)^k}{\partial f_1}\Delta f_1^k+\\ \dfrac{\partial\left(p_m^*\right)^k}{\partial f_2}\Delta f_2^k+\\ \dfrac{\partial\left(p_m^*\right)^k}{\partial f_3}\Delta f_3^k-1\end{array}\right)\frac{\partial\left(p_m^*\right)^k}{\partial f_2}\right]=0 \quad \text{(A13)}$$

$$\sum_{m=1}^{5}\left[\left(\begin{array}{l}\left(p_m^*\right)^k+\dfrac{\partial\left(p_m^*\right)^k}{\partial f_1}\Delta f_1^k+\\ \dfrac{\partial\left(p_m^*\right)^k}{\partial f_2}\Delta f_2^k+\\ \dfrac{\partial\left(p_m^*\right)^k}{\partial f_3}\Delta f_3^k-1\end{array}\right)\frac{\partial\left(p_m^*\right)^k}{\partial f_3}\right]=0 \quad \text{(A14)}$$

Equations A12, A13, and A14 are next rearranged as

$$\sum_{m=1}^{5}\left[\frac{\partial\left(p_m^*\right)^k}{\partial f_1}\frac{\partial\left(p_m^*\right)^k}{\partial f_1}\right]\Delta f_1^k+$$

$$\sum_{m=1}^{5}\left[\frac{\partial\left(p_m^*\right)^k}{\partial f_1}\frac{\partial\left(p_m^*\right)^k}{\partial f_2}\right]\Delta f_2^k+$$

$$\sum_{m=1}^{5}\left[\frac{\partial\left(p_m^*\right)^k}{\partial f_1}\frac{\partial\left(p_m^*\right)^k}{\partial f_3}\right]\Delta f_3^k=$$

$$-\sum_{m=1}^{5}\left[\frac{\partial\left(p_m^*\right)^k}{\partial f_1}\left(\left(p_m^*\right)^k-1\right)\right] \quad \text{(A15)}$$

$$\sum_{m=1}^{5}\left[\frac{\partial\left(p_m^*\right)^k}{\partial f_2}\frac{\partial\left(p_m^*\right)^k}{\partial f_1}\right]\Delta f_1^k + \sum_{m=1}^{5}\left[\frac{\partial\left(p_m^*\right)^k}{\partial f_2}\frac{\partial\left(p_m^*\right)^k}{\partial f_2}\right]\Delta f_2^k + \sum_{m=1}^{5}\left[\frac{\partial\left(p_m^*\right)^k}{\partial f_2}\frac{\partial\left(p_m^*\right)^k}{\partial f_3}\right]\Delta f_3^k = -\sum_{m=1}^{5}\left[\frac{\partial\left(p_m^*\right)^k}{\partial f_2}\left(\left(p_m^*\right)^k-1\right)\right] \quad \text{(A16)}$$

$$\sum_{m=1}^{5}\left[\frac{\partial\left(p_m^*\right)^k}{\partial f_3}\frac{\partial\left(p_m^*\right)^k}{\partial f_1}\right]\Delta f_1^k + \sum_{m=1}^{5}\left[\frac{\partial\left(p_m^*\right)^k}{\partial f_3}\frac{\partial\left(p_m^*\right)^k}{\partial f_2}\right]\Delta f_2^k + \sum_{m=1}^{5}\left[\frac{\partial\left(p_m^*\right)^k}{\partial f_3}\frac{\partial\left(p_m^*\right)^k}{\partial f_3}\right]\Delta f_3^k = -\sum_{m=1}^{5}\left[\frac{\partial\left(p_m^*\right)^k}{\partial f_3}\left(\left(p_m^*\right)^k-1\right)\right] \quad \text{(A17)}$$

Equations A15, A16, and A17 can be expressed in matrix form as

$$[S]\{\Delta f^k\} = -\{S^*\} \quad \text{(A18)}$$

where

$$[S]=\begin{bmatrix} S_{11} & S_{12} & S_{13} \\ S_{21} & S_{22} & S_{23} \\ S_{31} & S_{32} & S_{33} \end{bmatrix} =$$

$$\begin{bmatrix} \sum_{m=1}^{5}\frac{\partial\left(p_m^*\right)^k}{\partial f_1}\frac{\partial\left(p_m^*\right)^k}{\partial f_1} & \sum_{m=1}^{5}\frac{\partial\left(p_m^*\right)^k}{\partial f_1}\frac{\partial\left(p_m^*\right)^k}{\partial f_2} \\ \sum_{m=1}^{5}\frac{\partial\left(p_m^*\right)^k}{\partial f_1}\frac{\partial\left(p_m^*\right)^k}{\partial f_3} & \sum_{m=1}^{5}\frac{\partial\left(p_m^*\right)^k}{\partial f_2}\frac{\partial\left(p_m^*\right)^k}{\partial f_1} \\ \sum_{m=1}^{5}\frac{\partial\left(p_m^*\right)^k}{\partial f_2}\frac{\partial\left(p_m^*\right)^k}{\partial f_2} & \sum_{m=1}^{5}\frac{\partial\left(p_m^*\right)^k}{\partial f_2}\frac{\partial\left(p_m^*\right)^k}{\partial f_3} \\ \sum_{m=1}^{5}\frac{\partial\left(p_m^*\right)^k}{\partial f_3}\frac{\partial\left(p_m^*\right)^k}{\partial f_1} & \sum_{m=1}^{5}\frac{\partial\left(p_m^*\right)^k}{\partial f_3}\frac{\partial\left(p_m^*\right)^k}{\partial f_2} \\ \sum_{m=1}^{5}\frac{\partial\left(p_m^*\right)^k}{\partial f_3}\frac{\partial\left(p_m^*\right)^k}{\partial f_3} & \end{bmatrix} \quad \text{(A19)}$$

and

$$\left\{S^*\right\}=\begin{Bmatrix} S_1^p \\ S_2^p \\ S_3^p \end{Bmatrix} = \begin{Bmatrix} \sum_{m=1}^{5}\frac{\partial\left(p_m^*\right)^k}{\partial f_1}\left(\left(p_m^*\right)^k-1\right) \\ \sum_{m=1}^{5}\frac{\partial\left(p_m^*\right)^k}{\partial f_2}\left(\left(p_m^*\right)^k-1\right) \\ \sum_{m=1}^{5}\frac{\partial\left(p_m^*\right)^k}{\partial f_3}\left(\left(p_m^*\right)^k-1\right) \end{Bmatrix}$$

$$\left\{\Delta f^k\right\}=\begin{Bmatrix} \Delta f_1^k \\ \Delta f_2^k \\ \Delta f_3^k \end{Bmatrix} \quad \text{(A20, A21)}$$

Thus, Equations A1, A2, and A3 are modified to equation A18 where the three unknown incremental terms $\Delta f_1^k$, $\Delta f_2^k$, and $\Delta f_3^k$ are explicitly defined in terms of the known quantities. The solution of $\Delta f_1^k$, $\Delta f_2^k$, and $\Delta f_3^k$ are used next to obtain $f_1^{k+1}$, $f_2^{k+1}$, and $f_3^{k+1}$ (expression A5) that are employed to compute $(p_m^c)^{k+1}$ using the numerical heat transfer and fluid flow model. Next, $O(f)^{k+1}$ is calculated as

$$O(f)^{k+1}=\sum_{m=1}^{5}\left(\left(p_m^*\right)^{k+1}-1\right)^2 \quad \text{(A22)}$$

Values of $f_1$, $f_2$, and $f_3$ are assumed to reach optimum when the calculated value of $O(f)^{k+1}$ is smaller than a predefined small number. For the two dependent variables $p_m^*$ and $w_m^*$, Equation A19 is modified as

$$[S]=\begin{bmatrix} S_{11} & S_{12} & S_{13} \\ S_{21} & S_{22} & S_{23} \\ S_{31} & S_{32} & S_{33} \end{bmatrix} \quad \text{(A23)}$$

where

$$S_{ij}=\sum_{m=1}^{5}\left(\frac{\partial\left(p_m^*\right)^k}{\partial f_i}\frac{\partial\left(p_m^*\right)^k}{\partial f_j}+\frac{\partial\left(w_m^*\right)^k}{\partial f_i}\frac{\partial\left(w_m^*\right)^k}{\partial f_j}\right) \text{ for } i,j=1 \text{ to } 3 \quad \text{(A24)}$$

Equation A20 will be modified as

$$\left\{S^*\right\}=\begin{Bmatrix} S_1^{pw} \\ S_2^{pw} \\ S_3^{pw} \end{Bmatrix} = \begin{Bmatrix} \sum_{m=1}^{5}\left(\frac{\partial\left(p_m^*\right)^k}{\partial f_1}\left(\left(p_m^*\right)^k-1\right)+\frac{\partial\left(w_m^*\right)}{\partial f_1}\left(\left(w_m^*\right)^k-1\right)\right) \\ \sum_{m=1}^{5}\left(\frac{\partial\left(p_m^*\right)^k}{\partial f_2}\left(\left(p_m^*\right)^k-1\right)+\frac{\partial\left(w_m^*\right)}{\partial f_2}\left(\left(w_m^*\right)^k-1\right)\right) \\ \sum_{m=1}^{5}\left(\frac{\partial\left(p_m^*\right)^k}{\partial f_3}\left(\left(p_m^*\right)^k-1\right)+\frac{\partial\left(w_m^*\right)}{\partial f_3}\left(\left(w_m^*\right)^k-1\right)\right) \end{Bmatrix} \quad \text{(A25)}$$

Equations A5 and A21 do not change since the number of unknown parameters remains three. Furthermore, the sensitivity terms such as

$$\frac{\partial\left(p_m^*\right)^k}{\partial f_i} \text{ or } \frac{\partial\left(w_m^*\right)^k}{\partial f_i} \quad \text{(for i = 1 to 3)}$$

in Equation A18 often tend to be very small as the values of the unknown parameters $f_1$, $f_2$ and $f_3$ move close to the optimum. As a result, the matrix [S] tends to become singular. To avoid numerical instability, Equation A18 is further modified following the LM method as

$$\left([S]+\lambda I\right)\left\{\Delta f^k\right\}=-\left\{S^*\right\} \quad \text{(A26)}$$

where $\lambda$ is a scalar damping coefficient, usually about 0.001, and I is a diagonal matrix given by (Ref. 42)

$$I=\begin{bmatrix} S_{11} & 0 & 0 \\ 0 & S_{22} & 0 \\ 0 & 0 & S_{33} \end{bmatrix} \quad \text{(A27)}$$

The product $\lambda 1$ in Equation A26 ensures that the left-hand term in Equation A26 will remain nonzero even if the determinant of the matrix [S] is zero. The value of $\lambda$ is usually increased or decreased by a factor of ten as the value of the objective function in subsequent iterations increases or decreases. This, in effect, ensures the reduction or enhancement in step size as the solution respectively tends to diverge or converge. The algorithm of the complete procedure using the LM method can be presented as follows:

Step 1. Guess initial values (e.g., $k^{th}$) of unknown variables set, $\{f_i^k\}$ for i=1, 3 from Equation 12.

Step 2. Choose initial value of damping factor ($\lambda$).

Step 3. Compute the value of the objective function, $O(f^k)$ from Equation 11.

Step 4. Solve for the set of unknown in-

crements $\{\Delta f_i^k\}$ for i = 1, 3 from Equation A26.

Step 5. Compute $\{f_i^{k+1}\}$ for i = 1, 3 from Equation A5.

Step 6. Compute $O(f^{k+1})$ from Equation 11.

Step 7. If $O(f^{k+1}) \geq O(f^k)$, set $\lambda = 10\,\lambda$; reject $\{f_i^{k+1}\}$; go back to step 4.

Step 8. If $O(f^{k+1}) < O(f^k)$, set $\lambda = 0.1\,\lambda$.

Step 9. Exit if $O(f^{k+1}) - O(f^k)$ " $\varepsilon_1$ and $\{f_i^{k+1}\} - \{f_i^k\}$ " $\varepsilon_2$; or go back to step 4. $\varepsilon_1$ and $\varepsilon_2$ are two small, predefined numbers.

## Appendix 2

Considering the objective function defined in Equation 11 with two dependent variables, $p_m^*$ and $w_m^*$, and three unknown parameters, $f_1$, $f_2$, and $f_3$, Equation 17 can be written as

$$f_1^{k+1} = f_1^k - \beta^k d_1^k$$
$$f_2^{k+1} = f_2^k - \beta^k d_2^k$$
$$f_3^{k+1} = f_3^k - \beta^k d_3^k \qquad \text{(A28)}$$

where $f_1^{k+1}$, $f_2^{k+1}$, $d_1^k$, $d_2^k$, and $\beta^k$ confirm to their definitions presented previously. In Equation 18, as $O(f_i)^{k+1}$ contains $(p_m^*)^{k+1}$ and $(w_m^*)^{k+1}$ obtained from numerical heat transfer and fluid flow code using values of $f_1^{k+1}$, $f_2^{k+1}$, and $f_3^{k+1}$, and $O(f_i)^{k+1}$ depends on $f_1^{k+1}$, $f_2^{k+1}$, and $f_3^{k+1}$. Thus, replacing $(f_i)^{k+1}$ in Equation 18 by $f_1^{k+1}$, $f_2^{k+1}$, and $f_3^{k+1}$, and substituting the right-hand side of Equation A28 in place of them, Equation 18 can be rewritten as

$$\frac{\partial O\left(\begin{matrix} f_1^k - \beta^k d_1^k, f_2^k - \\ \beta^k d_2^k, f_3^k - \beta^k d_3^k \end{matrix}\right)}{\partial \beta^k} = 0;\ \beta^k \geq 0 \qquad \text{(A29)}$$

Considering two dependent variables, and $p^*_m$, $w^*_m$, $O\left(f_1^k - \beta^k d_1^k, f_2^k - \beta^k d_2^k, f_3^k - \beta^k d_3^k\right)$ can be expressed further as

$$O\left(f_1^k - \beta^k d_1^k, f_2^k - \beta^k d_2^k, f_3^k - \beta^k d_3^k\right)$$
$$\equiv \sum_{m=1}^{5}\left[p_m^*\left(f_1^k - \beta^k d_1^k, f_2^k - \beta^k d_2^k, f_3^k - \beta^k d_3^k\right) - 1\right]$$
$$+ \sum_{m=1}^{5}\left[w_m^*\left(f_1^k - \beta^k d_1^k, f_2^k - \beta^k d_2^k, f_3^k - \beta^k d_3^k\right) - 1\right] \qquad \text{(A30)}$$

Substituting Equation A30 in Equation A29 and using Taylor's expansion, Equation A29 can be substantially rearranged to give $\beta^k$ as (Refs. 41, 42)

$$\beta^k = \frac{\sum_{m=1}^{5}\left\{\begin{bmatrix}\left(p_m^* - 1\right)\left(\frac{\partial p_m^*}{\partial f_1^k} d_1^k + \frac{\partial p_m^*}{\partial f_2^k} d_2^k + \frac{\partial p_m^*}{\partial f_3^k} d_3^k\right)\end{bmatrix} + \begin{bmatrix}\left(w_m^* - 1\right)\left(\frac{\partial w_m^*}{\partial f_1^k} d_1^k + \frac{\partial w_m^*}{\partial f_2^k} d_2^k + \frac{\partial w_m^*}{\partial f_3^k} d_3^k\right)\end{bmatrix}\right\}}{\sum_{m=1}^{5}\begin{bmatrix}\left(\frac{\partial p_m^*}{\partial f_1^k} + \frac{\partial w_m^*}{\partial f_1^k}\right) d_1^k + \left(\frac{\partial p_m^*}{\partial f_2^k} + \frac{\partial w_m^*}{\partial f_2^k}\right) d_2^k + \left(\frac{\partial p_m^*}{\partial f_3^k} + \frac{\partial w_m^*}{\partial f_3^k}\right) d_3^k\end{bmatrix}^2} \qquad \text{(A31)}$$

Furthermore, following Equation 13, Equations 20a and 20b can respectively be rewritten as

$$\gamma^k = \frac{\sum_{i=1}^{3}\sum_{m=1}^{5}\left\{\left(p_m^* - 1\right)\frac{\partial p_m^*}{\partial f_i^k} + \left(w_m^* - 1\right)\frac{\partial w_m^*}{\partial f_i^k}\right\}^2}{\sum_{i=1}^{3}\sum_{m=1}^{5}\left\{\left(p_m^* - 1\right)\frac{\partial p_m^*}{\partial f_i^{k-1}} + \left(w_m^* - 1\right)\frac{\partial w_m^*}{\partial f_i^{k-1}}\right\}^2} \qquad \text{(A32)}$$

$$\gamma^k = \frac{\sum_{i=1}^{3}\sum_{m=1}^{5}\left[\begin{bmatrix}\left\{\left(p_m^* - 1\right)\frac{\partial p_m^*}{\partial f_i^k} + \left(w_m^* - 1\right)\frac{\partial w_m^*}{\partial f_i^k}\right\}\end{bmatrix}\begin{bmatrix}\left\{\left(p_m^* - 1\right)\left(\frac{\partial p_m^*}{\partial f_i^k} - \frac{\partial p_m^*}{\partial f_i^{k-1}}\right) + \left(w_m^* - 1\right)\left(\frac{\partial w_m^*}{\partial f_i^k} - \frac{\partial w_m^*}{\partial f_i^{k-1}}\right)\right\}\end{bmatrix}\right]}{\sum_{i=1}^{3}\sum_{m=1}^{5}\left\{\left(p_m^* - 1\right)\frac{\partial p_m^*}{\partial f_i^{k-1}} + \left(w_m^* - 1\right)\frac{\partial w_m^*}{\partial f_i^{k-1}}\right\}^2} \qquad \text{(A33)}$$

for k = 1, 2 and, $\gamma^0 = 0$. Apart from the calculation of conjugate coefficient, $\gamma^k$, both CGPR and CGFR methods are the same.